Flow Turbulence Combust (2016) 96:693–716
DOI 10.1007/s10494-015-9657-6

Assessment of Five SGS Models for Low-Re_m MHD Turbulence

Amar KC[1] · Abhilash J. Chandy[1]

Received: 25 March 2015 / Accepted: 26 September 2015 / Published online: 10 October 2015

Abstract Assessment of three regularization-based and two eddy-viscosity-based subgrid-scale (SGS) turbulence models for large eddy simulations (LES) are carried out in the context of magnetohydrodynamic (MHD) decaying homogeneous turbulence (DHT) with a Taylor scale Reynolds number (Re_λ) of 120 and a MHD transition-to-turbulence Taylor-Green vortex (TGV) problems with a Reynolds number of 3000, through direct comparisons to direct numerical simulations (DNS). Simulations are conducted using the low-magnetic Reynolds number approximation ($Re_m << 1$). LES predictions using the regularization-based Leray-α,LANS-α, and Clark-α SGS models, along with the eddy viscosity-based non-dynamic Smagorinsky and the dynamic Smagorinsky models are compared to in-house DNS for DHT and previous results for TGV. With regard to the regularization models, this work represents their first application to MHD turbulence. Analyses of turbulent kinetic energy decay rates, energy spectra, and vorticity fields made between the varying magnetic field cases demonstrated that the regularization models performed poorly compared to the eddy-viscosity models for all MHD cases, but the comparisons improved with increase in magnitude of magnetic field, due to a decrease in the population of SGS eddies within the flow field.

Keywords LES · SGS modeling · Taylor Green vortex · MHD turbulence

1 Introduction

Several technological and industrial applications, like steel production and processing involve the flow of electrically conducting fluids under the influence of a magnetic field[18].

✉ Abhilash J. Chandy
achandy@uakron.edu

Amar KC
ak139@zips.uakron.edu

[1] Department of Mechanical Engineering, University of Akron, Akron, OH 44325-3903, USA

In such applications, magnetic Reynolds number, Re_m defined as

$$Re_m = U_o L_o / \eta_m \tag{1}$$

is very small, i.e. $Re_m \ll 1$. The physical significance of such a regime is that there is a one-way coupling between fluctuations of the magnetic field and velocity, which allows considering the electromagnetic effect as an additional body force in the momentum equations of the flow. On the other end of the spectrum, $Re_m \geq 1$ and the coupling is now two-way. Applications of this regime include astrophysics and geophysics [16, 19].

A feature of low-Re_m magnetohydrodynamic (MHD) turbulence is that a strong magnetic field makes the turbulent fluctuations anisotropic, resulting in an elongation of the flow structures along the lines of the magnetic field [3, 35]. A fully-resolved numerical solution of the Navier-Stokes equations is called direct numerical simulation (DNS), which is inapplicable to very high-Reynolds number (Re) flows due to the increased computational expense. Large eddy simulation (LES) overcomes this limitation by filtering out all scales of motion larger than a cutoff filter width, Δ, while the scales smaller than Δ are represented using subgrid-scale (SGS) models [38].

Homogeneous MHD turbulence forms an ideal platform to illustrate how an applied magnetic field, while introducing anisotropy in the flow, can also increase the decay rate. Several studies involving DNS of homogeneous MHD turbulence have been conducted concentrating both on forced turbulence [6, 46, 47] and decaying turbulence [1, 7, 30, 32, 33]. Some of these works also included LES, focusing on SGS modeling in the context of MHD turbulence [1, 30, 32, 33]. With regard to SGS modeling, Knaepen and Moin [33] showed that the dynamic Smagorinsky model performed better than the classical non-dynamic Smagorinsky model. More recently Burattini *et al.* carried out a numerical investigation of MHD turbulence at magnetic interaction parameter values ranging from 0 to 50 [7]. They found that nonlinearity dominated the flow evolution and hence a linear theory could not describe the flow.

In the last two decades, various SGS models have been developed [45]. For instance, implicit LES [27] is an LES approach where no SGS model is employed and the numerical effects of the discretization are assumed to mimic the physics of unresolved turbulent motion. The second and the most widely-used approach is the eddy viscosity kind (e.g. the Smagorinsky model) [38, 42, 44], that requires a model for the anisotropic residual stress tensor term to close the equations for the filtered velocity. A more novel approach involves regularization modeling as a SGS model (e.g. the Leray-α model) [15, 23, 24]. These models are based on smoothing the dynamics of Navier-Stokes equations [24] via a direct modification of the nonlinear convection terms, while still retaining the mathematical properties of the equations [25]. As a result they differ from the eddy-viscosity models in that they result in a mixed formulation involving both the filtered and unfiltered solution [24].

In this paper, we considered three regularization models including the Leray-α, LANS-α and Clark-α. In the Leray-α model, the advective operator of Navier-Stokes (NS) equations, $(u \cdot \nabla)u$ is replaced by $(v \cdot \nabla)u$, where the filtered velocity, $v = H^{-1}(u)$, and H is the Helmholtz filter. Reeuwijk et al. [39] compared the Leray-α simulations from well resolved and coarse DNS and concluded that additional dissipative modeling was needed to capture accurately all the effects from turbulence. Another approach is the Lagrangian averaged Navier-Stokes-α (LANS-α) model equations (also referred to as the Casmassa-Holm equation) [12–14]. Different comparisons for LANS-α have been made to DNS at modest Taylor-scale Reynolds number for decaying ($Re_\lambda = 130$ [14], $Re_\lambda = 220$ [36], $Re_\lambda = 300$ [15]) and forced turbulence ($Re_\lambda = 80$ and 115, [36]). The comparisons presented in [23]

between Leray-α and LANS-α showed that the LANS-α model provided a solution that represented the filtered DNS results better. The third and final regularization model considered here is the Clark-α model [17]. A study of Graham et al. [26] has compared the three regularization models (Leray-α, LANS-α and Clark-α) with DNS for a high-Re Taylor-Green forced isotropic turbulence problem and found that Clark-α produced the best dissipation rate and energy spectrum at scales larger than α. They also showed how the LANS-α model performed the best in terms of predicting intermittency. A study by one of the co-authors also compared these three regularization models for high-Re homogeneous turbulence and Taylor-Green vortex [9]. The study found that all the regularization models performed better at high-Re when additional dissipation was included. More recently, another investigation by the co-author [11], compared the Leray-α model to DNS for low-Re_m MHD turbulence and found that the former was unable to predict the energy transfer and anisotropy accurately.

The performance of the five different SGS models is presented for LES of low-Re_m MHD turbulence and comparisons are made to an in-house DNS results from [11] at varying magnetic field strengths (different values of magnetic interaction parameter, N). In addition to the three regularization models described above, the classical non-dynamic and dynamic Smagorinsky models are also tested. Two different cases are considered here: The first is a homogeneous turbulence case, while the second the Taylor-Green vortex (TGV) case. TGV is a simple system that is very useful to study the generation of small scales and the turbulence resulting from it [5]. Decay rates, energy spectra, and vortical structures are analyzed at varying values of N. In the subsequent sections, the formulation, computational details and SGS models are described and this is followed by the presentation and discussion of results obtained.

2 Formulation

The formulation employed in the current study is based on the Fourier pseudo-spectral method that integrates the incompressible Navier-Stokes equations in a cubic box of side L for periodic boundary conditions:

$$\begin{aligned} \partial_t \mathbf{u} + (\mathbf{u}\cdot\nabla)\mathbf{u} &= -\nabla p + \nu\nabla^2\mathbf{u} + \mathbf{f} \\ \nabla\cdot\mathbf{u} &= 0 \end{aligned} \tag{2}$$

where $\mathbf{u}$, p, t and ν are the velocity field, pressure, time, and kinematic viscosity, respectively. The Lorentz force, $\mathbf{f}$ is given by:

$$\mathbf{f} = \frac{1}{\rho}\mathbf{J}\times\mathbf{B}, \tag{3}$$

$$\mathbf{J} = \sigma\left(-\nabla\phi + \mathbf{u}\times\mathbf{B}\right), \tag{4}$$

$$\nabla\cdot\mathbf{J} = 0, \tag{5}$$

and

$$\nabla\cdot\mathbf{B} = 0, \tag{6}$$

where $\mathbf{B}$, $\mathbf{J}$, σ, and ϕ represent the applied magnetic field, electric current density, electrical conductivity and the electrostatic potential, respectively. Ohm's law is represented by Eq. 4. Due to the fact that at low-Re_m, the magnetic field affects the flow, but not vice-versa, the Lorentz force term, $\mathbf{J}\times\mathbf{B}/\rho$ in the above equation is a function of only $\mathbf{B}$ and $\mathbf{u}$, where ρ is the density of the fluid. The magnetic field is assumed to be directed along the z direction.

So $\mathbf{B} = B_o\hat{k}$, where B_o is the amplitude of the magnetic field . Therefore, the Lorentz force term is linearly dependent on velocity [35, 43, 46] and is given by

$$\mathbf{f} = -\frac{\sigma B_o^2}{\rho}\nabla^{-2}\frac{\partial^2 \mathbf{u}}{\partial z^2} \tag{7}$$

A description of the current formulation is provided in [9, 11]. With the velocity field, $\mathbf{u}(\mathbf{x}, t)$, approximated as a finite Fourier series

$$\mathbf{u}(\mathbf{x}, t) = \sum_{\boldsymbol{k}} e^{i\boldsymbol{k}\cdot\mathbf{x}}\,\hat{\mathbf{u}}(\boldsymbol{k}, t), \tag{8}$$

where $\hat{(..)}$ is a variable in the spectral or fast Fourier transform (FFT) space, and $\boldsymbol{k}$ is the wavenumber vector, the incompressible Navier-Stokes equations in wavenumber space are:

$$\left(\frac{d}{dt} + \nu k^2 + \frac{\sigma B_o^2}{\rho}\left(\frac{k_z}{k}\right)^2\right)\hat{u}_j(\boldsymbol{k}, t) = -ik_l\left(\delta_{jk} - \frac{k_j k_k}{k^2}\right)\sum_{\boldsymbol{k'}}\hat{u}_k(\boldsymbol{k'}, t)\,\hat{u}_l(\boldsymbol{k} - \boldsymbol{k'}, t) \tag{9}$$

where σ, $\boldsymbol{k}$ and i are the resistivity, wavenumber vector, and the imaginary unit, respectively, and $k \equiv |\boldsymbol{k}|$. For details on the quasi static derivation, see [40]. So the electromagnetic force in the above governing equations represents an anisotropic term in the equation of motion. From the above governing equations, a non-dimensional parameter, namely the interaction parameter, N, can be defined as

$$N = \frac{\sigma B_o^2 L_o}{\rho U_o}. \tag{10}$$

N represents the strength of the magnetic damping term relative to convection in Eq. 9 and also the ability of a magnetic field to reduce 3D turbulence to 2D turbulence.

2.1 SGS models

2.1.1 Two eddy-viscosity models

The classical Smagorinsky model [44] assumes quasi-equilibrium between large and small scales. Here, the filtered Navier-Stokes equation yields,

$$\partial_i \tilde{u}_i = 0 \tag{11}$$

$$\partial_t \tilde{u}_i + \tilde{u}_j\partial_j\tilde{u}_i = -\partial_i\tilde{p} + \nu\partial_{jj}\tilde{u}_i - \partial_j\tau_{ij,R} + f_i \tag{12}$$

where $\tilde{(.)}$ is the LES-filtered quantity and the residual stress is

$$\tau_{ij,R} = -2\nu_T\tilde{S}_{ij} = -2(C_s\Delta)^2\,|\,\tilde{\mathbf{S}}\,|\,\tilde{S}_{ij} \tag{13}$$

where Δ is the filter width and C_s is the Smagorinsky model coefficient, which is determined independent of the specific filter. For isotropic turbulence in the inertial range, C_s is fixed at its classical value, $C_s = 0.16$ [38], and $\tilde{S}_{ij} = \frac{1}{2}(\partial_j\tilde{u}_i + \partial_i\tilde{u}_j)$ is the resolved strain-rate tensor with a magnitude of $|\tilde{\mathbf{S}}| = (2\tilde{S}_{mn}\tilde{S}_{mn})^{1/2}$. This model allows only forward energy transfer from the resolved scales to the subgrid scales.

For the dynamic Smagorinsky model, the filtered Navier-Stokes are written in the same manner as presented above for the non-dynamic Smagorinsky, except now the model coefficient, C_s, for calculating the residual stress, is calculated as,

$$C_s^2 = \frac{\langle L_{ij}\,M_{ij}\rangle}{\langle M_{ij}\,M_{ij}\rangle} \tag{14}$$

where $\langle\ .\ \rangle$ is a volume-averaged quantity. From the Germano identity [22],

$$L_{ij} \equiv T_{ij} - \bar{\tau}_{ij} = \overline{\tilde{u}_i \tilde{u}_j} - \bar{\tilde{u}}_i \bar{\tilde{u}}_j \tag{15}$$

where $\bar{(.)}$ is a test-filtered quantity on a filter width of 2Δ, $T_{ij} = \overline{\widetilde{u_i u_j}} - \bar{\tilde{u}}_i \bar{\tilde{u}}_j$ is the SGS tensor [29], and

$$M_{ij} \equiv -2\Delta^2 \Big[4 \mid \bar{\tilde{\mathbf{S}}} \mid \bar{\tilde{S}}_{ij} - \overline{\mid \tilde{\mathbf{S}} \mid \tilde{S}_{ij}} \Big]. \tag{16}$$

2.1.2 Three regularization models

The different regularization models considered here are, Leray-α, LANS-α and Clark-α. The governing equations in the Leray formulation can be written as,

$$\partial_i u_i = 0, \quad \partial_i v_i = 0 \tag{17}$$

$$\partial_t u_i + v_j \partial_j u_i = -\partial_i p + \nu \partial_{jj} u_i + f_i \tag{18}$$

where the flow is advected by a smoothed (filtered) velocity $\boldsymbol{v}$.

$$v = H^{-1} u = (1 - \alpha^2 \nabla)^{-1} u. \tag{19}$$

H is the Helmholtz filter and α is the Helmholtz length, which defines the effective width of the filter. H is the standard filter used for all the regularization models considered here. Similarly, for the LANS-α model and the Clark-α models, Eq. 17 stays the same, but Eq. 18 is replaced by

$$\partial_t u_i + v_j \partial_j u_i + u_j \partial_i v_j = -\partial_i p + \nu \partial_{jj} u_i + f_i \tag{20}$$

and

$$\partial_t u_i + \partial_j (v_j u_i + u_j v_i - v_j v_i - \alpha^2 \partial_l u_i \partial_l u_j) = -\partial_i p + \nu \partial_{jj} u_i + f_i, \tag{21}$$

respectively.

3 Computational Details

The computer code solving the pseudo-spectral equations described above is written in Fortran90 and employs the P3DFFT parallel three-dimensional FFT library. See the authors' recent publications [9–11] and thesis [31], for more details. The 3/2-rule is used as the dealiasing technique [41]. Grid resolutions illustrated in this paper for the different simulations are numbers after dealiasing. Temporal integration is achieved via a third-order Runge-Kutta time stepping algorithm [8]. $h = L/N_f$ is the numerical grid size, where N_f is the number of Fourier modes and $L = 2\pi$ is the side of the cubic computational domain. The time step, Δt, is calculated according to $\Delta t = (cfl)\ (h)/\sqrt{tke_0}$. In this equation, tke_0 is the initial turbulent kinetic energy, and cfl=0.03 [38] for all the cases presented here. Also, the time step size is set to be a constant throughout the simulation. The total simulation time was 10.0 in the case of homogeneous turbulence and 20.0 in the case of Taylor-Green vortex.

4 Results

In this section the results from five different SGS models such as the non-dynamic Smagorinsky (NDSMAG), Dynamic Smagorinsky (DSMAG), Leray-α (LERAY), LANS-α

Table 1 Simulation parameters for DNS and SGS models

Cases	Grid	N	Filter width, Δ	Constants	Time step
DNS-MHD_N	256^3	0, 0.1, 0.5, 1	-	-	6×10^{-4}
LES: NDSMAG_N	96^3	0, 0.1, 0.5, 1	$\pi/48$	$\alpha = 1/42$, $C_s = 0.16$	5.3×10^{-3}
LES: DSMAG_N	96^3	0, 0.1, 0.5, 1	$\pi/48$	$\alpha = 1/42$	5.3×10^{-3}
LES: LERAY_N	96^3	0, 0.1, 0.5, 1	$\pi/48$	$\alpha = 1/42$	5.3×10^{-3}
LES: LANS_N	96^3	0, 0.1, 0.5, 1	$\pi/48$	$\alpha = 1/42$	5.3×10^{-3}
LES: CLARK_N	96^3	0, 0.1, 0.5, 1	$\pi/48$	$\alpha = 1/42$	5.3×10^{-3}

(LANS) and Clark-α (CLARK) are compared with in-house DNS results [9] for homogeneous MHD turbulence and previous simulations for the TGV case [4, 5]. The value of α is taken as 1/42, which gives the best agreement compared to $\alpha > 1/42$ and there is no significant difference in the results by decreasing the value of $\alpha < 1/42$ [9]. These models presented here are compared with DNS results without a magnetic field, i.e. $N = 0$ and with a magnetic field using values of $N = 0.1, 0.5$ and 1. For all the simulations presented here, the magnetic filed is applied only in the z-direction.

In the case of non-dynamic Smagorinsky model, the constant C_s is fixed at 0.16, which is the conventional value for isotropic turbulence [34]. Simulation parameters for both the homogeneous MHD turbulence and MHD Taylor-Green vortex are presented in Table 1.

4.1 Homogeneous turbulence

The first problem considered here is that of an initially-isotropic decaying turbulence case of Taylor scale Reynolds number, $Re_\lambda = 120$. The Taylor length scale and the r.m.s. velocity in the longitudinal direction are used to calculate Re_λ, i.e. $Re_\lambda = u_{1r.m.s.}\nu/\lambda$, where ν is the viscosity. DNS and LES were both initialized was with a divergence-free velocity field and an energy spectrum according to [38] given by

$$E(k) = C_k \epsilon^{2/3} k^{-5/3} \left(\frac{kL_u}{[(kL_u)^2 + c_L]^{1/2}} \right)^{5/3+p_0} \exp\left(-\beta\{[(k\eta)^4 + c_\eta^4]^{1/4} - c_\eta\} \right). \quad (22)$$

k is the wavenumber, L_u is the integral length scale and is 0.6, and η, the Kolmogorov length scale, is given by

$$\eta = Re_L^{-3/4} L_u = 1.8937. \quad (23)$$

In the above equation, Re_L is the integral scale Reynolds number given by

$$Re_L = 3\ Re_\lambda^2\ /20 = 2160 \quad (24)$$

In the energy spectrum function, p_0, c_L, and c_η are constants given by 2.0, 3.75, and 0.4, respectively [21, 38]. In addition, the constants, $C_k = 1.5$ and $\beta = 5.2$, values chosen such that the total turbulent kinetic energy associated with the initial velocity field is 0.55. The initialization is based on the process outlined in [29], where the velocity field is scale in Fourier space using random phase Fourier modes, such that the energy spectrum represents the initial energy spectrum. Using these initial conditions, the simulations are run for a certain time period (2.0, here), such that the velocity derivative skewness remains steady, after which the velocity field is rescaled in Fourier space so that the initial energy distribution is matched at this state and the time is reset to $t = 0$.

Figure 1 shows the comparison of turbulent kinetic energy (TKE) evolution for the five different SGS models with DNS results. TKE of filtered turbulence (filtered using spectral cutoff filter) is obtained by integrating the 3D energy spectrum according to,

$$TKE = \int_0^{k_{max}} E(k)dk$$

where k_{max} is the largest wavenumber represented by, $k_{max} = \pi N/L = \pi/\Delta x$. L is the side of the domain, Δx is the grid spacing and N is the grid size. A spectral-cutoff filter with the same LES filter width size is used to truncate the DNS data, so that o that direct comparisons can be made with the LES-filtered TKE. Essentially, the spectral cutoff filter is an implicit numerical grid filter of filter size, $\Delta = h$ in a pseudo-spectral code. So for a LES grid resolution of 96^3 after dealiasing, like the one employed in this paper, the filter size, Δ, is $\pi/48$.

The LES calculations for the different models are compared with in-house DNS results for four different values of N, $N = 0, 0.1, 0.5$ and 1 in Fig. 1. Obviously the TKE decreases

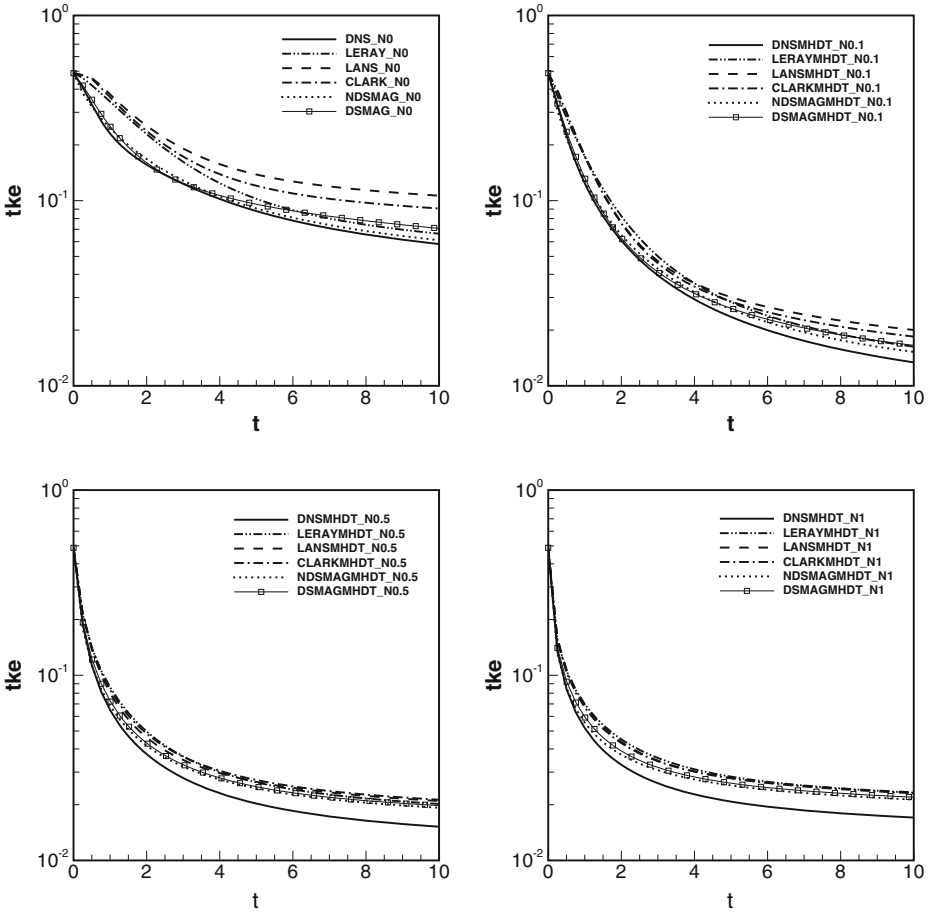

Fig. 1 Evolution of the TKE with time, for five different SGS models compared with DNS, with different values of N. N0, N0.1, N0.5, N1 represent $N = 0, 0.1, 0.5$ and 1, respectively

with time because of decaying turbulence, but it decreases faster with increasing magnetic field due to the Joule dissipation effects resulting from the magnetic Lorentz force. With regard to the performance of the SGS models, in the absence of magnetic field, the Smagorinsky models seem to predict the TKE evolution better than the regularization models. All the regularization models overpredict the TKE at all times, with the LANS-α being the worst. It is interesting to note that with an increase in magnetic field, the agreement between the regularization models and the DNS results keeps improving until at $N = 1$, all the SGS models are quite close to each other and do a reasonably good job in predicting the evolution of TKE. Furthermore, in order to quantify the deviations of all the SGS models from DNS, evolution of the ratio of TKE values between the SGS models and DNS, given by $\text{tke}_{\text{SGS}}/\text{tke}_{\text{DNS}}$, is plotted for the different magnetic fields in Fig. 2. For the DNS calculations these values would be one, since there is no SGS model present. The overestimation of TKE at all times for all magnetic fields is clear from the larger-than-one values of this ratio. In addition, the SGS models are the most different from each other, with time, for the case

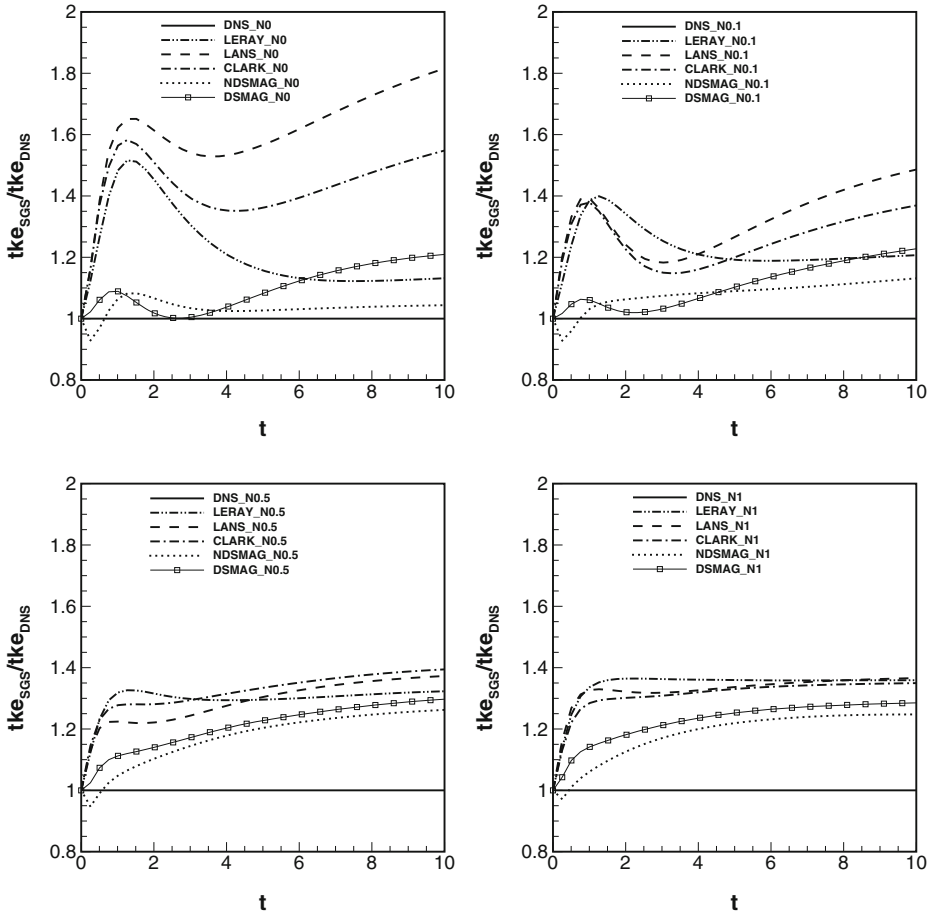

Fig. 2 Evolution of the ratio of SGS TKE to the DNS TKE, with time, for five different SGS models compared with DNS, with different values of N. N0, N0.1, N0.5, N1 represent N = 0, 0.1, 0.5 and 1, respectively

of no magnetic field. As the magnetic field increases, the models tend to be closer to each other and to the DNS. Overall, as was seen previously in Fig. 1, the Smagorinsky models fare better than the regularization models, with the non-dynamic Smagorinsky model performing marginally better than its dynamic counterpart. Among the regularization models, the Leray model does the best, followed by Clark and then LANS.

Comparisons for the evolution of decay rate of TKE are presented in Fig. 3. In order to emphasize the behavior at early times, results are presented for a time of $t < 4$ and also again on a log-linear scale. The TKE decay rate increases early ($t < 0.3$) and subsequently decreases. For the no-magnetic field case, the Smagorinsky models are better than the regularization models, with the dynamic Smagorinsky doing a slightly better job. All the regularization models show a delay in the peak and also severely underpredict the peak of the TKE decay rate. With an increase in magnetic field, the comparisons are better with DNS results, with the SGS models all on top of DNS for the $N = 1$ case. The kind of behavior observed in the plots of TKE and TKE decay rate shows again, how the regularization

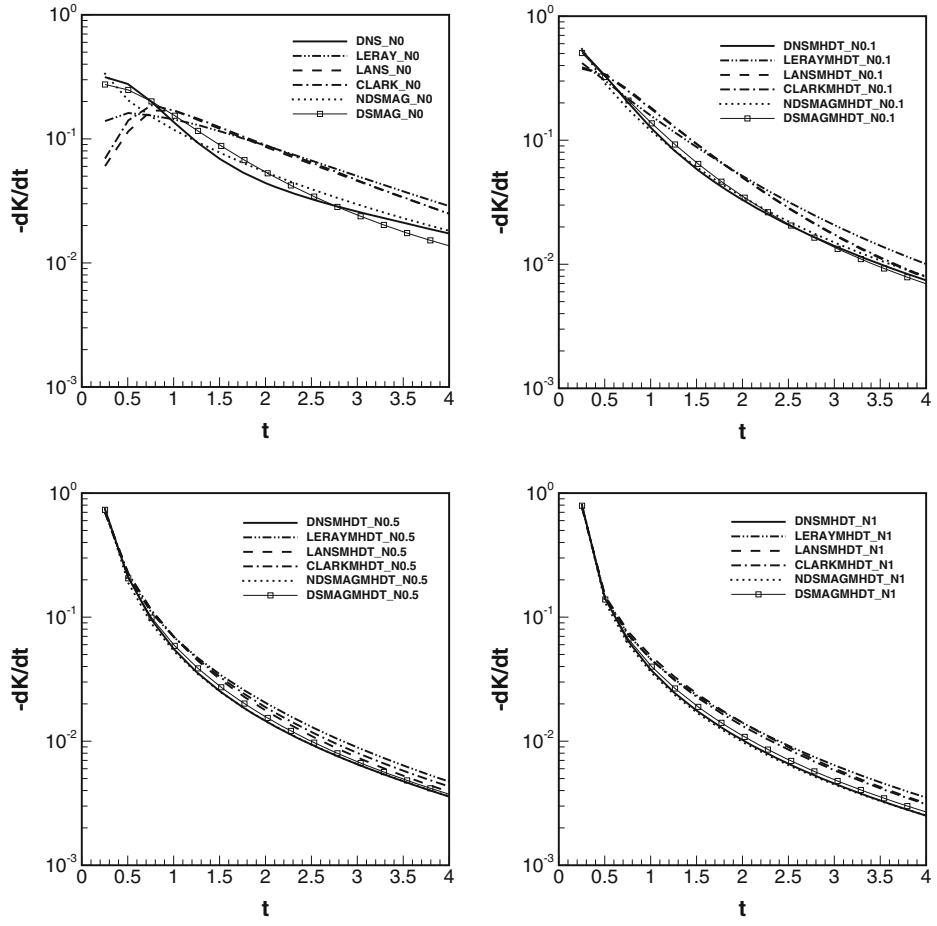

Fig. 3 Evolution of rate of decay of TKE, dK/dt, with time, for five different SGS models compared with DNS; with different values of N. N0, N0.1, N0.5, N1 represent $N = 0$, 0.1, 0.5 and 1, respectively

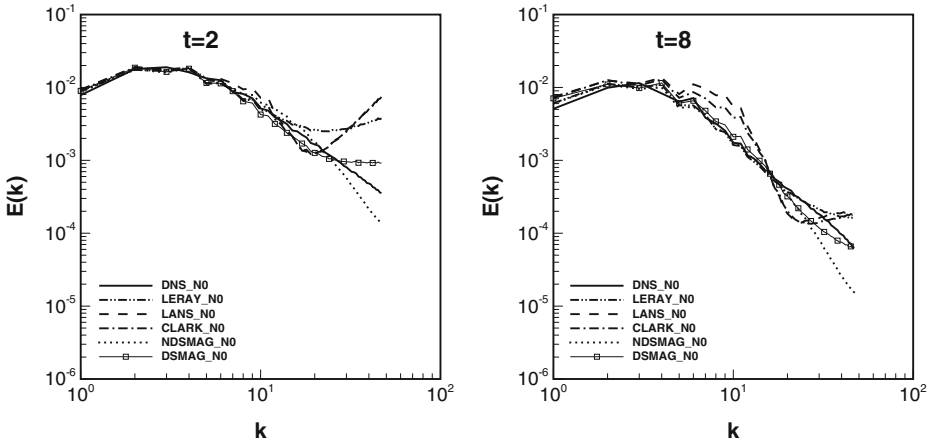

Fig. 4 Spectra, E(k), at two different times; N0 represents magnetic interaction parameter, $N = 0$

models are unable to correctly predict the energy levels at high-Re. But when the magnetic field is added, the effective Re is reduced [3] resulting in better predictions compared to DNS. This was also seen in some of the author's recent works [11].

The energy distributed across the entire range of scales can be illustrated through energy spectra and it gives a better and more specific understanding of the ability of the SGS models to correctly predict the energy with regard to the different length scales. In one of the author's earlier works [11], the effect of a SGS model was presented for homogeneous turbulence in the absence of magnetic field by comparing the $3D$ energy spectra of the Leray-α model to low- or LES-resolution DNS calculations. Figures 4 – 7 show the 3D energy spectra for the various magnetic field cases at two different times, $t = 2$ and $t = 8$. Consider the $N = 0$ case, where the magnetic field is absent. Here, all the SGS models compare well with DNS for the low-wavenumbers or large length scales at both the times. But early in the simulation ($t = 2$), at the high-wavenumbers ($\mathbf{k} > 20$) or small length scales, there is an

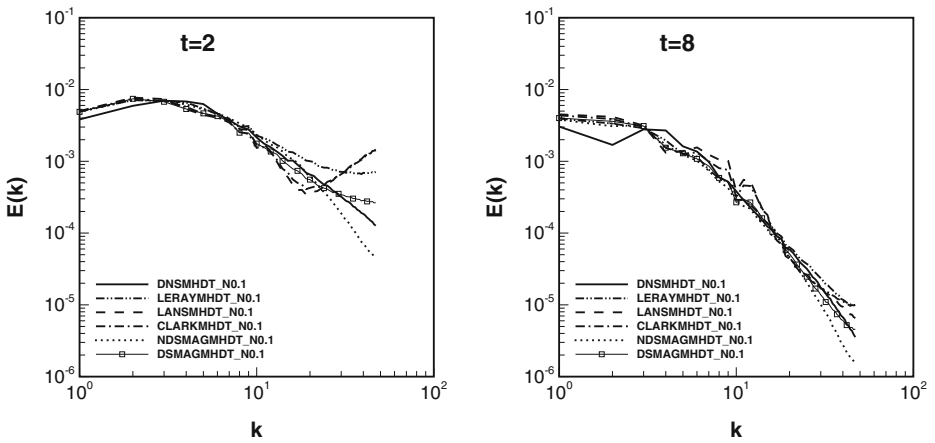

Fig. 5 Spectra, E(k), at two different times; N0.1 represents magnetic interaction parameter, $N = 0.1$

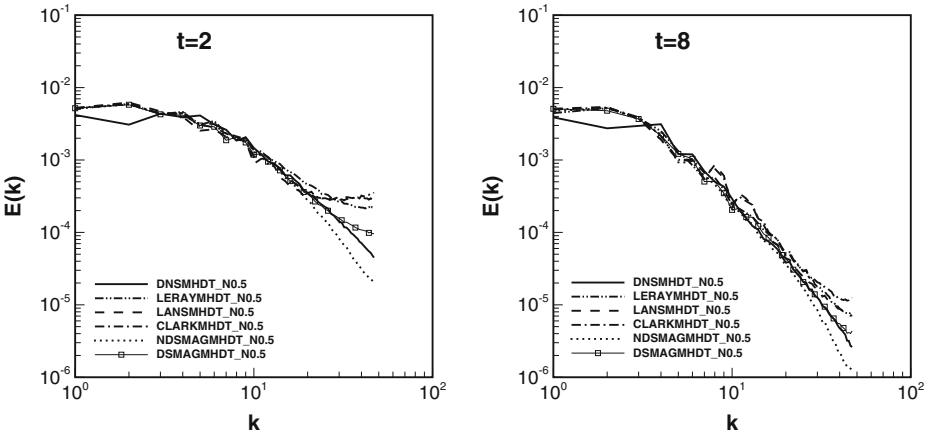

Fig. 6 Spectra, E(k), at two different times; N0.5 represents magnetic interaction parameter, $N = 0.5$

insufficient dissipation of energy resulting in a build-up at these wavenumbers. This phenomena was exhibited only to a slight extent by the dynamic Smagorinsky model, but for the regularization models, discrepancy was much worse. With regard to the non-dynamic Smagorinsky model, no build-up of energy can be seen. In fact it underpredicts the energy at the small scales, but such a behavior is a function of the Smagorinsky constant, C_s, whose value was chosen as 0.16 in these simulations. Later at $t = 8$ the comparisons are better with DNS, with only slight build-up observed at the high wavenumbers. But that is because at this stage of the simulation, the small-scales have dissipated significantly and hence the SGS models, especially the regularization models are able to predict the energy levels better at this stage.

To assess the scaling of the spectra at the different times and different magnetic fields, compensated spectra, $Ec = \epsilon^{-2/3}k^{5/3}E(k)$ is plotted in Fig. 8 for two different times, but only for two magnetic field cases, $N = 0$ and $N = 0.5$. With the inertial subrange approximately being when $3 \leq k \leq 8$, it can be seen that the $5/3$ scaling only holds at early

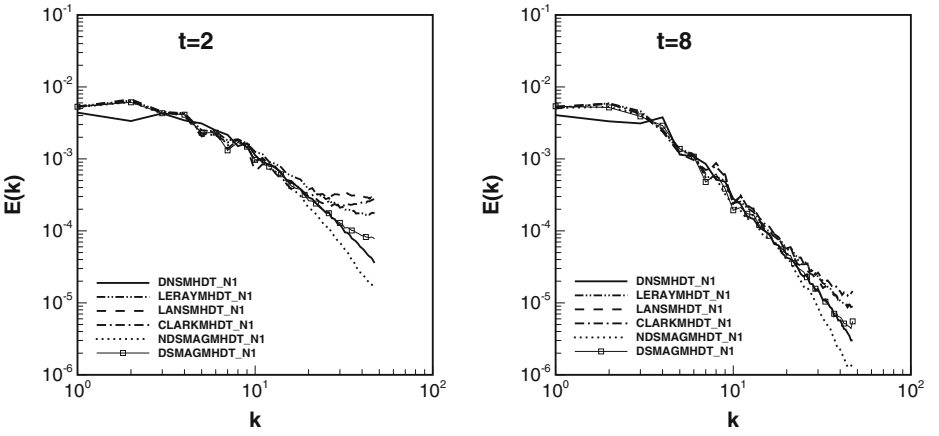

Fig. 7 Spectra, E(k), at two different times; N1 represents magnetic interaction parameter, $N = 1$

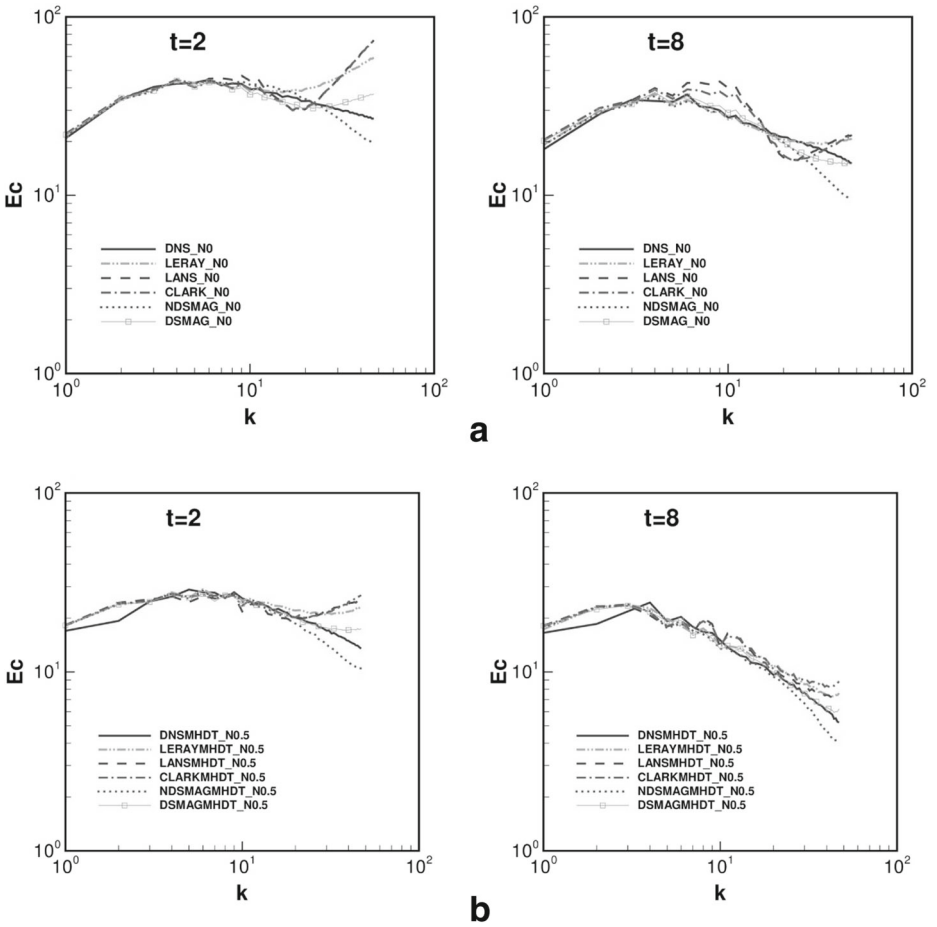

Fig. 8 Compensated spectra, $Ec = \epsilon^{-2/3}k^{5/3}E(k)$, at two different times; (**a**) N0 represents magnetic interaction parameter, $N = 0$ and (**b**) N0.5 represents magnetic interaction parameter, $N = 0.5$

times for both the magnetic field cases and all SGS models. At a later time of $t = 8$ for the no-magnetic field case, only DNS exhibits a $5/3$ scaling, albeit over a much shorter range of $3 \leq k \leq 5$. With regard to the $N = 0.5$ case, none of the models including DNS has a $5/3$ scaling. All of this behavior is expected, firstly, due to the fact that turbulence is decaying and the range over which any model would exhibit a $5/3$ scaling would just get shortened. Although, none of the SGS models seem to predict this correctly. Secondly, with the addition of the magnetic field, the turbulence is getting damped and the effect does become more pronounced with time as well. As a result, isotropic turbulence illustrated by a $5/3$ slope in the energy spectra along the inertial subrange cannot exist.

With the inclusion of magnetic field (See Figs. 5, 6 and 7), the Lorentz force comes into play, and the Joule dissipation from the magnetic field affects all modes including the more energetic large-scales, thus reducing their energy levels. The same phenomena is seen at the small scales too, due to a reduction in the energy cascade from large scales

to small scales [11]. Energy spectra for the magnetic field cases show a similar behavior as what was seen for $N = 0$, where the regularization models exhibit a larger build-up of energy at the small scales compared to the eddy-viscosity models. But the results do

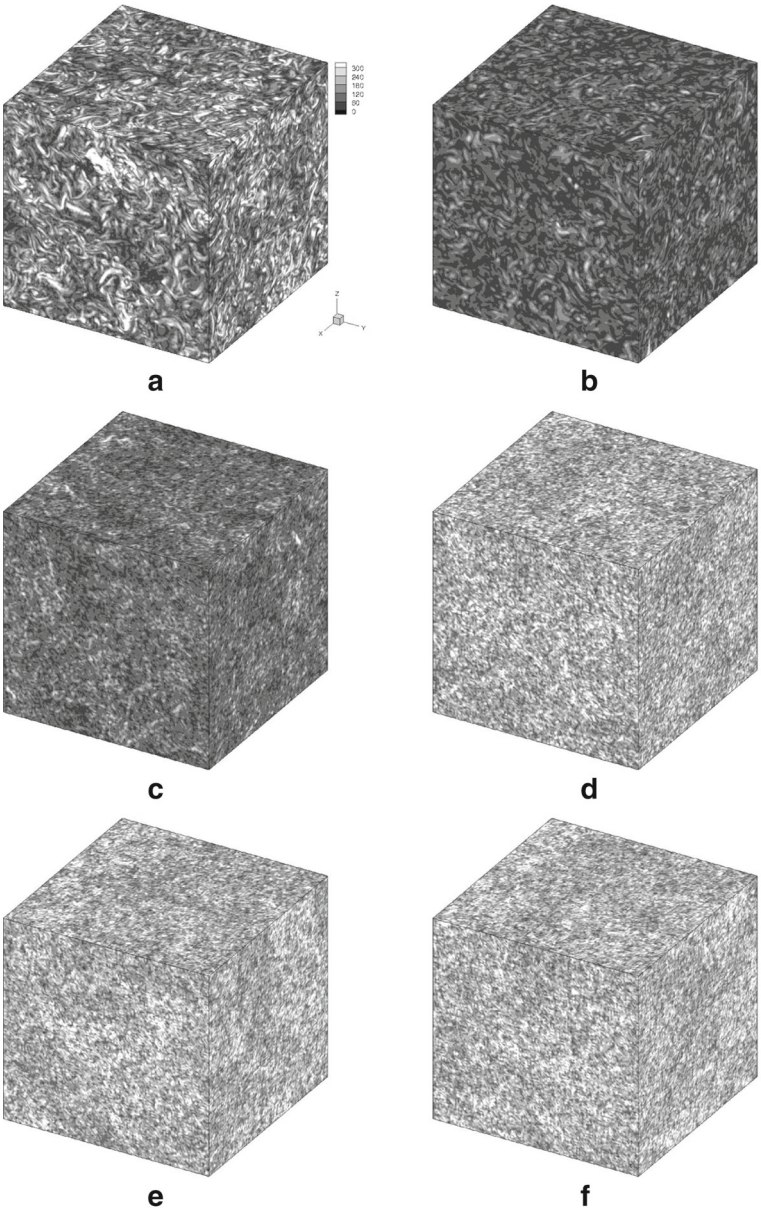

Fig. 9 3D Gray scale contours of vorticity magnitude at time, $t = 6$ for DNS and the different SGS models without magnetic field i.e. with a magnetic interaction parameter, $N = 0$; (**a**) DNS (**b**) NDSMAG(**c**) DSMAG (**d**) LERAY (**e**) LANS (**f**) CLARK. The legends and the axes for the contours are the same

show an overall improvement with increase in magnetic field. That is because the magnetic field tends to suppress the turbulent fluctuations, reduce the turbulent kinetic energy at all the scales and thereby reduce the level of turbulence itself (i.e. an overall reduction in effective Re).

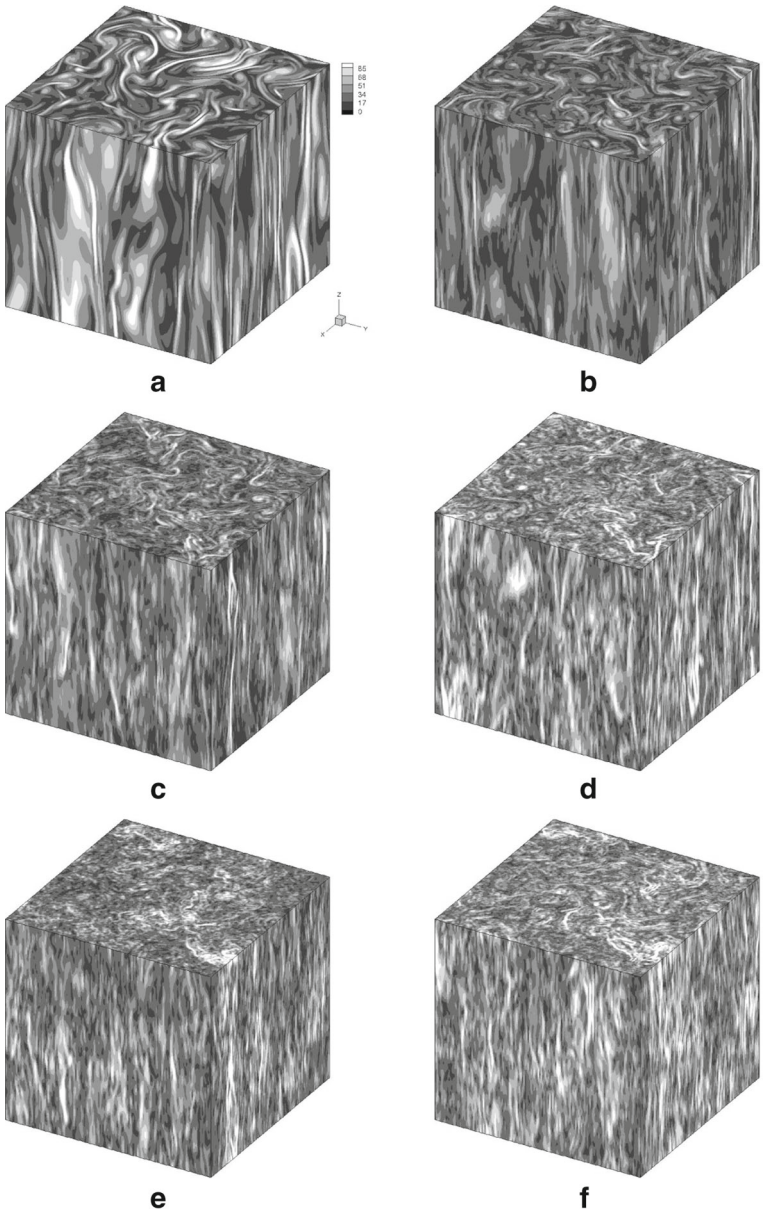

Fig. 10 3D Gray scale contours of vorticity magnitude at time, t = 6 s, for DNS and the different SGS models with a magnetic interaction parameter, N = 0.5; (**a**) DNS (**b**) NDSMAG (**c**) DSMAG (**d**) LERAY (**e**) LANS (**f**) CLARK. The legends and the axes for the contours are the same

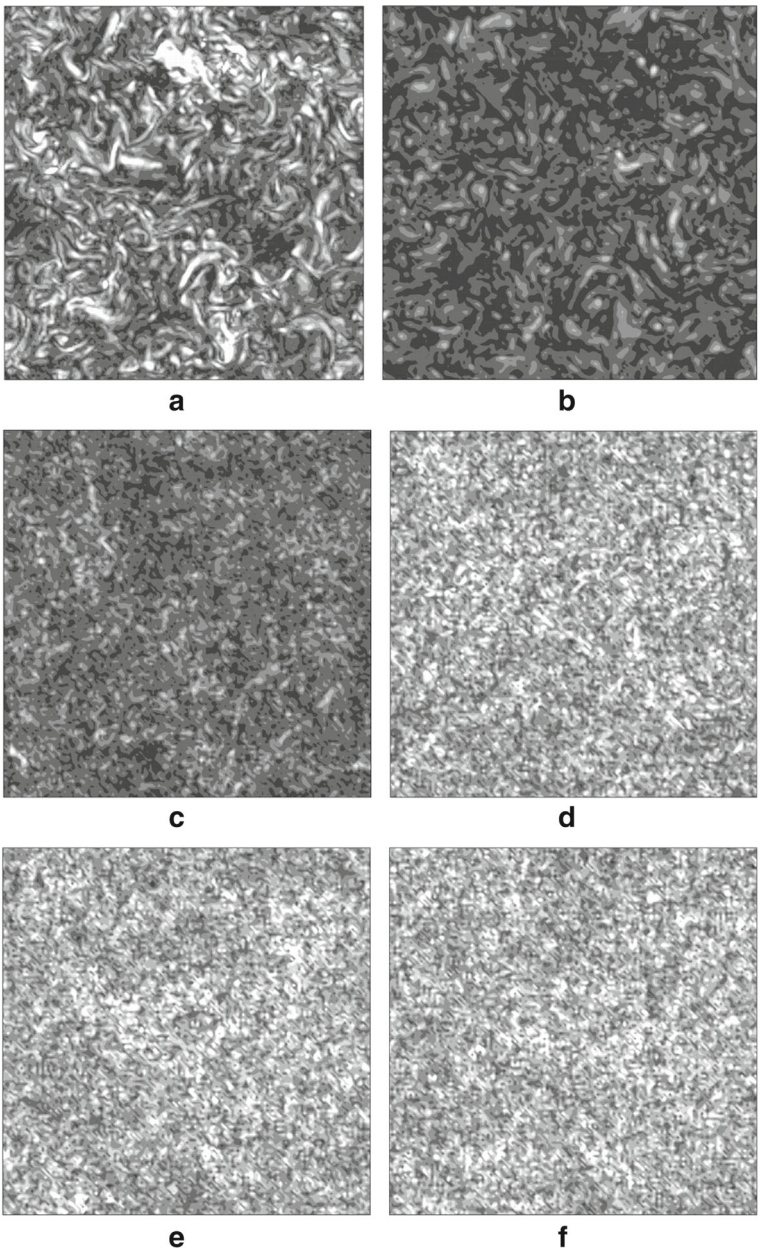

Fig. 11 2D Gray scale contours of vorticity magnitude on the $Y - Z$ plane at time, $t = 6$ for DNS and the different SGS models without magnetic field i.e. with a magnetic interaction parameter, $N = 0$; (**a**) DNS (**b**) NDSMAG (**c**) DSMAG (**d**) LERAY (**e**) LANS (**f**) CLARK. The legends and the axes for the contours are the same

To visualize the effect of anisotropy on the flow, 3D and 2D contours of vorticity magnitude are presented as gray scale contours for only two magnetic interaction parameters, $N = 0$ and $N = 0.5$, in Figs. 9–12, at time, $t = 6$ s, for the six (One DNS + five LES)

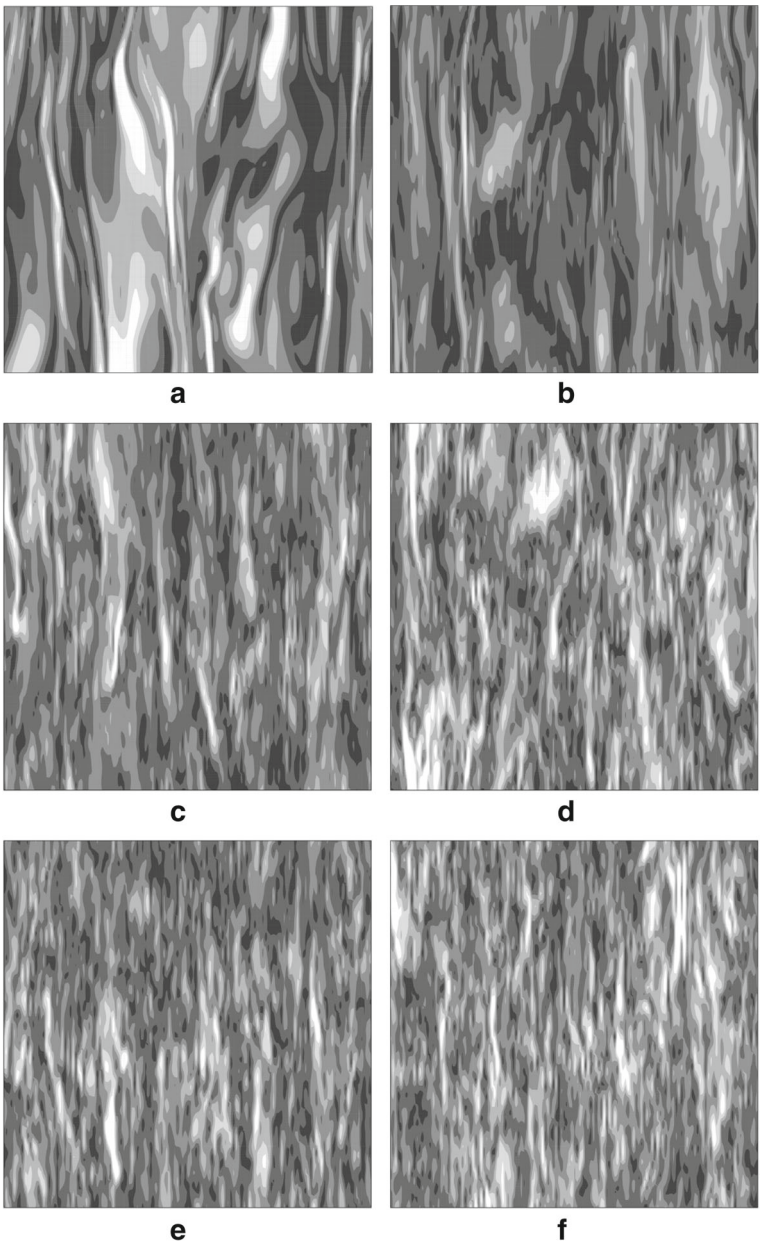

Fig. 12 2D Gray scale contours of vorticity magnitude on the $Y - Z$ plane at time, t = 6 s, for DNS and different SGS models with a magnetic interaction parameter, N = 0.5; (**a**) DNS (**b**) NDSMAG (**c**) DSMAG (**d**) LERAY (**e**) LANS (**f**) CLARK. The legends and the axes for the contours are the same

different cases in a π^3 domain. It can be seen from Fig. 10 that the flow becomes nearly two-dimensional in the $x - y$ plane with an increase in the magnetic field due to the damping of fluid motions in the direction of the magnetic field, i.e. the z-direction, thus causing a flow

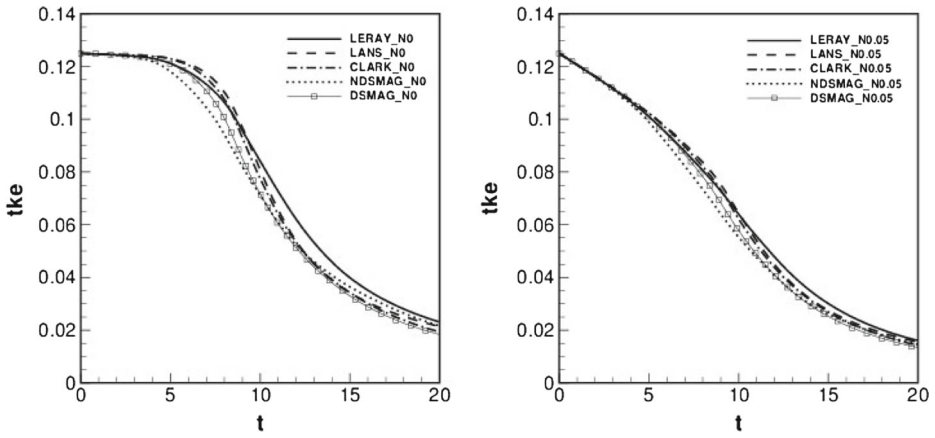

Fig. 13 Evolution of the TKE of TGV with time, for five different SGS models, with different values of N

stretching in the same direction. A center slice along the $Y - Z$ plane of the domain is presented in Figs. 11 and 12 and the two-dimensionality of the flow field is clearly evident due to the flow being stretched in the z direction. While all the SGS model results qualitatively are similar to DNS, the dynamic Smagorinsky shows the better comparison quantitatively as indicated by the levels of gray scale contours and all the regularization models do a much poorer job in predicting the vorticity contours correctly.

4.2 Taylor green vortex

The classic Taylor-Green vortex (TGV) problem [37] is considered next. This is a transition to turbulence problem, which has its $3D$ velocity field initialized in physical space according to

$$\begin{aligned} u_{1,0} &= \sin(x)\cos(y)\cos(z) \\ u_{2,0} &= -\cos(x)\sin(y)\cos(z) \\ u_{3,0} &= 0 \end{aligned} \tag{25}$$

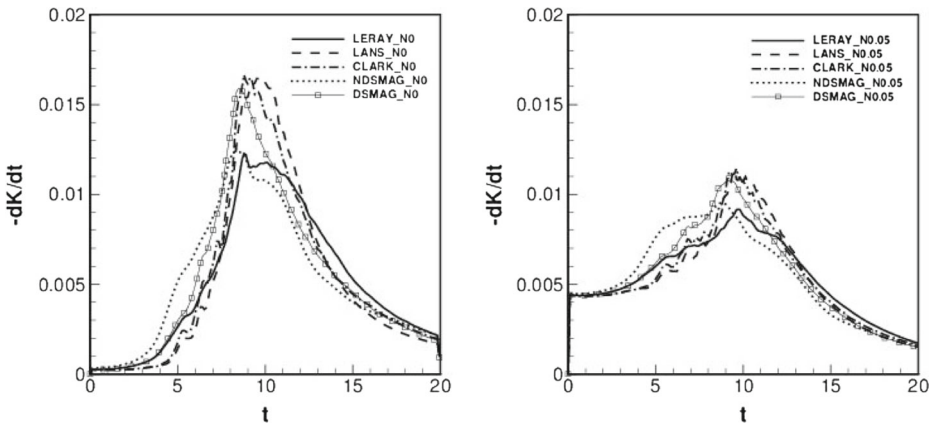

Fig. 14 Decay rate of TKE of TGV with time, for five different SGS models, with different values of N

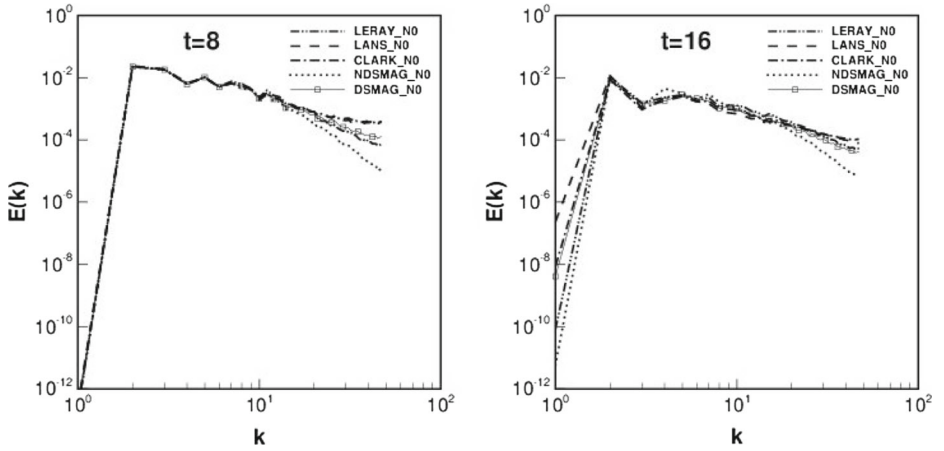

Fig. 15 Energy spectra, E(k), of TGV at two different times

A case of $Re = 3000$ is simulated here, where the Re is defined here as the inverse of the viscosity. There have been several studies in the past focusing on DNS [4, 5, 37] and LES [2, 20, 28], all in the absence of a magnetic field. To date, there haven't been any investigations related to a MHD TGV.

LES of the TGV is presented here for two different magnetic interaction parameters, $N = 0$ and $N = 0.05$, and for the five different SGS models: non-dynamic Smagorinsky (NDSMAG), dynamic Smagorinsky (DSMAG), Leray-α (LERAY), LANS-α (LANS) and Clark-α (CLARK). Figure 13 shows the evolution of the turbulent kinetic energy and Fig. 14 shows the evolution of the rate of energy decay. From the decay rate plots at $N = 0$, the results are qualitatively similar to previous results including DNS [4, 9], where the evolution follows two phases. In the first phase ($t < 9$), the flow essentially remains laminar and transitional, the flow structure would be highly organized and the dissipation increases from zero to a maximum value, as the flow turns turbulent. In the second phase ($t > 9$),

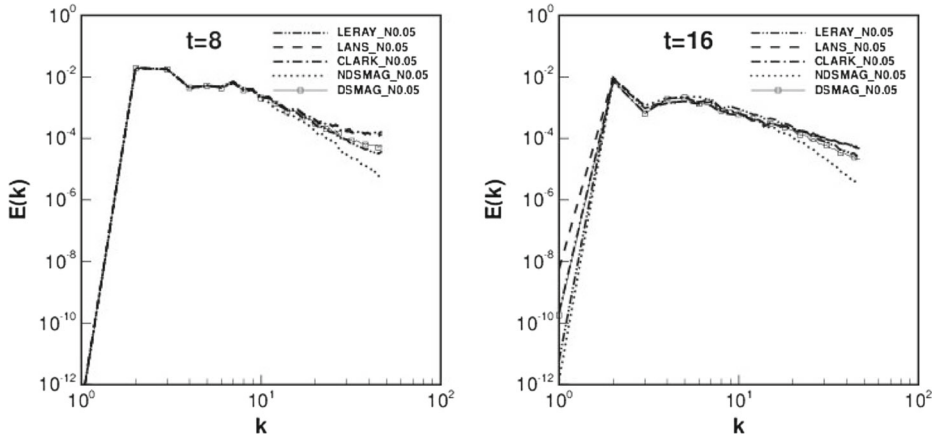

Fig. 16 Energy spectra, E(k), of TGV at two different times

starting with the maximum dissipation (or -dK/dt), the flow is of fully-developed turbulent nature and the dissipation keeps decreasing. From Fig. 13, it is clear that in general, with an increase in magnetic field, the energy decays faster due to the added Joule dissipation from the Lorentz force.

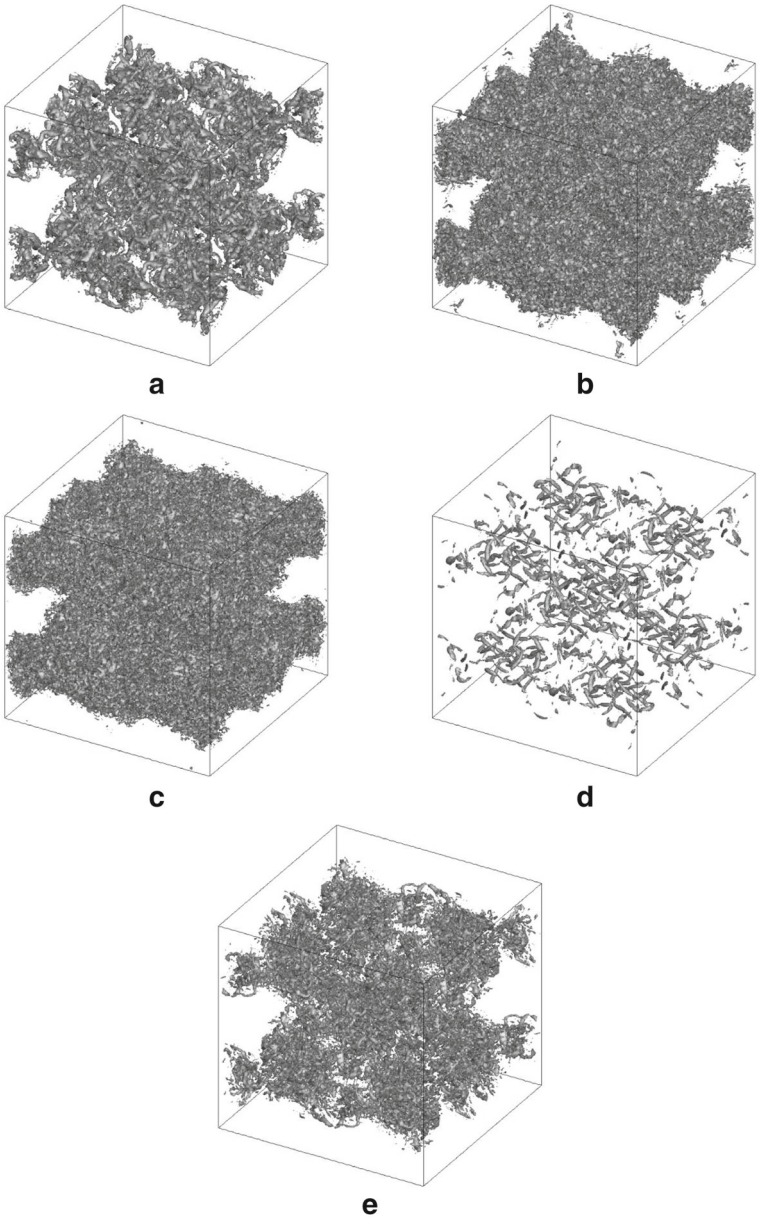

Fig. 17 Gray scale vortical structures at time, $t = 10$ in terms of iso-surfaces at $C = 12$ for the different SGS models without magnetic field i.e. with a magnetic interaction parameter, $N = 0$; (**a**) LERAY (**b**) LANS (**c**) CLARK (**d**) NDSMAG (**e**) DSMAG

In the no-magnetic field case, all the regularization models overpredict the *TKE* compared to the eddy-viscosity models mostly at all times, but in the presence of a magnetic field even as small as $N = 0.05$, the predictions are closer to each other. This is because the

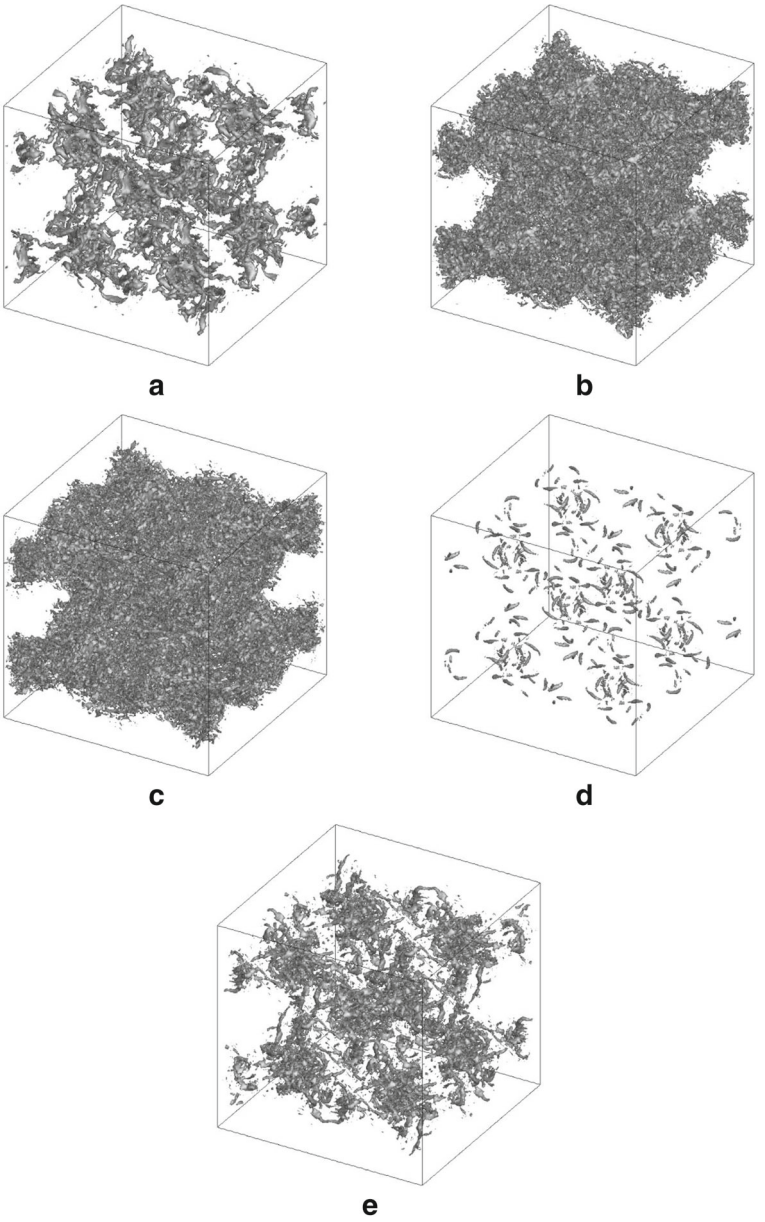

Fig. 18 Gray scale vortical structures at time, t = 10 s, in terms of iso-surface at value $C = 12$ for the different SGS models with a magnetic interaction parameter, N = 0.05; (**a**) LERAY (**b**) LANS (**c**) CLARK (**d**) NDSMAG (**e**) DSMAG

magnetic field has caused the flow to be less turbulent and the regularization models perform better in these conditions. With regard to the decay rate (in Fig. 14), the magnetic field has caused a delay in the transition to turbulence as indicated by all the SGS model results. And as expected the regularization models for reasons outlined previously, are closer to the Smagorinsky models.

Figures 15 and 16 show the energy spectra for the two magnetic field cases ($N = 0$ and $N = 0.05$) at two different times, $t = 8$ and $t = 16$. All the SGS models predict the large scales ($k < 20$) pretty well at all times and for both magnetic fields. With regard to the small scales ($k > 20$), compared to the dynamic Smagorinsky model, the non-dynamic Smagorinsky overpredicts the dissipation at all times and all magnetic field levels. On the other hand, the regularization models, especially the Leray-α and LANS-α tend to underpredict the dissipation, thereby displaying a build-up of energy at these large scales. The Clark-α model though is very close to the dynamic Smagorinsky for all the cases at all times. The predictions of the regularization models get better with time for a single magnetic field case and also with an increase in magnetic field because of the increased dissipation at the small scales at those conditions.

Figures 17 and 18 present the vortical structures in the form of iso-surfaces of vorticity magnitude at $C = 12$ for the different SGS models and the two magnetic field cases at $t = 10$ s. This time was chosen in order to indicate fully-developed turbulence. It can be seen that there are radical differences in the vortical structures between the regularization-type models and the eddy-viscosity models. The obvious difference is the amount of structures visible at this particular value. For instance, the non-dynamic Smagorinsky seems to show the least amount of structures, which is directly related to the overprediction of small-scale dissipation by this model. On the other end of the spectrum is the Leray model where it can be seen that the structures are thicker and more in the number, indicating the underprediction of dissipation. The LANS and Clark models also show much more structures compared to the Smagorinsky models, but smaller in size compared to the Leray model, indicating a level of predicted dissipation between Leray and Smagorinsky models.

5 Conclusions

A series of LES of low-Re_m MHD turbulence was examined in the context of a DHT case and the classic transition to turbulence case, the TGV. Five different SGS models such as the non-dynamic and dynamic Smagorinsky, which constitute eddy-viscosity-type models, and the Leray-α, LANS-α and Clark-α models which constitute the regularization-type models, were assessed for varying interaction parameters. The magnetic field was applied only in the z-direction and its strength was varied by varying values of the magnetic interaction parameter as, $N = 0, 0.05, 0.1, 0.5$, and 1. In the case of DHT, LES calculations conducted here were compared with in-house DNS.

For the decaying MHD turbulence calculations, comparisons with DNS for all the regularization models were worse than the Smagorinsky models, with the Leray-α performing the worst and the dynamic Smagorinsky the best. From the energy spectra it was clear that the regularization models underpredicted the dissipation at small scales indicating a build-up of energy due to insufficient resolution. On the other hand, the non-dynamic Smagorinsky did overpredict the dissipation, which could be related to the Smagorinsky constant chosen here in these studies ($C_s = 0.16$). The predictions of the regularization-based SGS models improved with increase in magnetic field though, due to a reduction in the effective Re as a result of the additional Lorentz force. In other words, the regularization models were

able to perform better with a decrease in the population of SGS eddies within the flow field. The vorticity contours in the box demonstrated how all the SGS models were able to qualitatively predict the stretching in the z-direction (due to the Lorentz force resulting from a z-direction magnetic field) reasonably well. However, with regard to actual vorticity values, the regularization model results did not match very well with the DNS, while the eddy-viscosity-based models fared better.

For the TGV case, only two magnetic field cases were simulated, $N = 0$ and $N = 0.05$ for a $Re = 3000$, because for values of $N > 0.05$, the flow remained almost frozen and there ceased to be any development towards turbulence in those cases. Qualitative comparisons were made with the DNS data from Brachet [4]. Again on assessing the five different SGS models, dynamic Smagorinsky seemed to perform the best and Leray the worst. All the SGS models predicted a further delay in transition to turbulence compared to the dynamic Smagorinsky as indicated by the decay rate evolution. The LANS and Clark models though did a better job in predicting the magnitudes of these decay rates while Leray and non-dynamic Smagorinsky highly underpredicted these values. The comparisons were closer to each other for the magnetic field case. The spectra demonstrated the same story as what was observed in homogeneous turbulence, where non-dynamic Smagorinsky showed too much dissipation at the small scales while the regularization models showed a build-up of energy at the small scales or the large wavenumbers, and again comparisons were better with an increased magnetic field. It was also interesting to note that the vortical structures characterized by iso-surfaces of vorticity magnitude also showed significant differences between the SGS models, especially with regard to the number of structures displayed at a particular value. For instance, the non-dynamic Smagorinsky showed the least amount of structures indicating the maximum dissipation, while regularization models showed the largest amount of structures indicating the least dissipation.

References

1. Agullo, O., Muller, W., Knaepen, B., Carati, D.: Large eddy simulation of decaying magnetohydrodynamic turbulence with dynamic subgrid-modeling. Phys. Plasmas **8**, 3502–3505 (2001)
2. Bensow, R., Larson, M., Vesterlund, P.: Vorticity-strain residual-based turbulence modelling of the Taylor-Green vortex. Int. J. Numer. Meth. Fluids **54**, 745–756 (2007)
3. Biskamp, D.: Magnetohydrodynamic Turbulence. Cambridge University Press, Cambridge (2003)
4. Brachet, M.E.: Direct numerical simulation of three-dimensional turbulence in Taylor-Green vortex. Fluid Dynamics Research **8**, 1–8 (1991)
5. Brachet, M.E., Meiron, D.I., Orszag, S.A., Nickel, B.G., Morf, R.H., Frisch, U.: Small scale structure of the Taylor-Green vortex. J. Fluid Mech. **130**, 411–452 (1983)
6. Burattini, P., Kinet, M., Carati, D., Knaepen, B.: Anisotropy of velocity spectra in quasistatic magnetohydrodynamic turbulence. Phys. Fluids **20**(165), 110 (2008)
7. Burattini, P., Zikanov, O., Knaepen, B.: Decay of magnetohydrodynamic turbulence at low magnetic Reynolds number. J. Fluid Mech **657**, 502–538 (2010)
8. Canuto, C., Hussaini, M.Y., Quarteroni, A., Zang, T.A.: Spectral methods in fluid dynamics. Springer-Verlag, New York (1987)
9. Chandy, A.J., Frankel, S.H.: Regularization-based sub-grid scale (sgs) models for large eddy simulations (les) of high-re decaying isotropic turbulence. J. Turbul. **10**(10) (2009)
10. Chandy, A.J., Frankel, S.H.: The t-model as a large eddy simulation model for Navier-Stokes equations. SIAM Multiscale Model Sim. J. **8**, 445–462 (2009)
11. Chandy, A.J., Frankel, S.H.: Leray-α les of magnetohydrodynamic turbulence at low magnetic Reynolds number. J. Turbul., N17 (2011)
12. Chen, S., Foias, C., Holm, D., Olson, E., Titi, E.: Wynne: A connection between the Camassa-Holm equations and turbulent flows in channels and pipes. Phys. Fluids **11**, 2343–2353 (1999)

13. Chen, S., Foias, C., Holm, D., Olson, E., Titi, E., Wynne, S.: Camassa-Holm equations as a closure model for turbulent channel and pipe flow. Phys. Rev. Let. **81**, 5338–5341 (1998)
14. Chen, S., Holm, D., Margolin, L.G., Zhang, R.: Direct numerical simulations of the Navier-Stokes alpha model. Phys. D Nonlinear Phenom **133**, 66–83 (1999)
15. Cheskidov, A., Holm, D., Olson, E., Edriss, S.T.: On a leray-α model of turbulence. Proc. Royal Soc. London, A **461**, 629–649 (2005)
16. Cho, J., Lazarian, A., Vishniac, E.: MHD turbulence: Scaling laws and astrophysical applications. Springer, New York (2003)
17. Clark, R.A., Ferziger, J.H., Reynolds, W.C.: Evaluation of subgrid-scale models using an accurately simulated turbulent flow. J. Fluid Mech. **91**, 1–16 (1979)
18. Davidson, P.: Magnetohydrodynamics in materials processing. Ann. Rev. Fluid. Mech. **31**, 273–285 (1999)
19. Davidson, P.: Introduction to Magnetohydrodynamics. Cambridge University Press, Cambridge (2001)
20. Drikakis, D., Fureby, C., Grinstein, F., Youngs, D.: Simulation of transition and turbulence decay in the Taylor-Green vortex. J. Turbulence **8**, 20 (2007)
21. Fox, R.O.: Computational models for turbulent reacting flows. Cambridge University Press (2003)
22. Germano, M., Piomelli, U., Moin, P., Cabot, W.H.: A dynamic subgrid-scale eddy viscosity model. Physics of Fluids A: Fluid Dynamics (1989-1993) **3**, 1760–1765 (1991)
23. Geurts, B.J.: Holm: Leray and LANS-α modelling of turbulent mixing. J. Turbulence **7**, 1–33 (2006)
24. Geurts, B.J., Holm, D.: Regularization modelling for large-eddy simulation. Phys. Fluids **15**, L13—L16 (2003)
25. Geurts, B.J., Kuczaj, A., Titi, E.: Regularization modelling for large-eddy simulation of homogeneous isotropic decaying turbulence. J. Phys. A: Math. Theor. **41**(344), 008 (2008)
26. Graham, J., Holm, D., Mininni, P., Pouquet, A.: Three regularization models of the Navier-Stokes equations. Phys. Fluids **20**(035), 107 (2008)
27. Grinstein, F.F., Margolin, L.G., Rider, W.J.: Implicit large eddy simulation: computing turbulent fluid dynamics. Cambridge University Press (2007)
28. Highes, T.: Multiscale phenomena: Green's functions, the Dirichlet-to-Neumann formulation, subgrid-scale models, bubbles and the origins of stabilized methods. Comput. Meth. Appl. Mech. Engg. **127**, 387–401 (1995)
29. Kang, H., Chester, S., Meneveau, C.: Decaying turbulence in an active-grid-generated flow and comparisons with large-eddy-simulation. J. Fluid Mech. **480**, 129–160 (2003)
30. Kassinos, S., Knaepen, B., Carati, D.: The transport of a passive scalar in magnetohydrodynamic turbulence subjected to mean shear and frame rotation. Phys. Fluids **19**(015), 105 (2007)
31. KC, A.: Numerical simulations of magnetohydrodynamic flow and heat transfer. University of Akron, Master's thesis (2014)
32. Knaepen, B., Kassinos, S., Carati, D.: Magnetohydrodynamic turbulence at moderate magnetic Reynolds number. J. Fluid Mech. **513**, 199–220 (2004)
33. Knaepen, B., Moin, P.: Large eddy simulation of conductive flows at low magnetic Reynolds number. Phys. Fluids **16**, 1255–1261 (2004)
34. Lilly, D.: The representation of small-scale turbulence in numerical simulation experiments. 320-1951, 195–210. Scientific Computing Symposium Environmental Sciences (1967)
35. Moffatt, H.: On the suppression of turbulence by a uniform magnetic field. J. Fluid Mech. **28**, 571–592 (1967)
36. Mohseni, K., Kosovic, B., Shkoller, S., Marsden, J.E.: Numerical simulations of the lagrangian averaged Navier-Stokes equations for homogenous isotropic turbulence. Phys. Fluids **15**, 524–544 (2003)
37. Orszag, S.A.: Numerical simulation of the Taylor-Green vortex. Lect. Notes Comput. Sci. **11**, 50–64 (1973)
38. Pope, S.B.: Turbulent Flows. Cambridge University Press, Cambridge (2000)
39. Reeuwijk, M.V., Jonker, H.J.J., Hanjali, K.: Incompressibility of the leray-α model for wall-bounded flows. Phys. Fluids **18**(018), 103 (2006)
40. Roberts, P.: An Introduction to Magnetohydrodynamics. Elsevier, New York (1967)
41. Rogallo, R.S.: Numerical experiments in homogeneous turbulence. NASA TM 81315, NASA (1981)
42. Sagaut, P. Large eddy simulation for incompressible flows: An introduction, Third Edition. Springer, New York (2006)
43. Schumann, U.: Numerical simulation of the transition from three- to two-dimensional turbulence under a uniform magnetic field. J. Fluid Mech. **74**, 31–58 (1976)
44. Smagorinsky, J.: General circulation experiments with the primitive equations. I. The basic experiment. Mon. Weather Rev. **91**(3), 99–164 (1963)

45. Su, M., Chen, Q., Chiang, C.M.: Comparison of different subgrid-scale models of large eddy simulation for indoor airflow modeling. J. Fluids Eng. **123**, 628–639 (2001)
46. Vorobev, A., Zikanov, O., Davidson, P., Knaepen, B.: Anisotropy of magnetohydrodynamic turbulence and low magnetic Reynolds number. Phys. Fluids **16**(125), 105 (2005)
47. Zikanov, O., Thess, A.: Direct numerical simulation of forces mhd turbulence at low magnetic Reynolds number. J. Fluid Mech. **358**, 299–333 (1998)